Quinacridone-Based Molecular Donors for Solution Processed Bulk-Heterojunction Organic Solar Cells

John Jun-An Chen,[‡,†] Teresa L. Chen,[‡,†] BongSoo Kim,[§,†] Daniel A. Poulsen,[§] Justin L. Mynar,[§] Jean M. J. Fréchet,[*,§,‡] and Biwu Ma[*,‡]

The Molecular Foundry, Lawrence Berkeley National Laboratory, Berkeley, California 94720, and College of Chemistry, University of California, Berkeley, California 94720

ABSTRACT New soluble quinacridone-based molecules have been developed as electron donor materials for solution-processed organic solar cells. By functionalizing the pristine pigment core of quinacridone with solubilizing alkyl chains and light absorbing/charge transporting thiophene units, i.e., bithiophene (BT) and thienylbenzo[c][1,2,5]thiadiazolethienyl (BTD), we prepared a series of multifunctional quinacridone-based molecules. These molecular donors show intense absorption in the visible spectral region, and the absorption range and intensity are well-tuned by the interaction between the quinacridone core and the incorporated thiophene units. The thin film absorption edge extends with the expansion of molecular conjugation, i.e., 552 nm for *N*,*N*′-di(2-ethylhexyl)quinacridone (**QA**), 592 nm for 2,9-Bis(5′-hexyl-2,2′-bithiophene)-*N*,*N*′-di(2-ethylhexyl)quinacridone (**QA-BT**), and 637 nm for 4-(5-hexylthiophen-2-yl)-7-(thiophen-2-yl)benzo[*c*][1,2,5]thiadiazole (**QA-BTD**). The change of molecular structure also influences the electrochemical properties. Observed from cyclic voltammetry measurements, the oxidation and reduction potentials (vs ferrocene) are 0.7 and −1.83 V for **QA**, 0.54 and −1.76 V for **QA-BT**, and 0.45 and −1.68 V for **QA-BTD**. Uniform thin films can be generated from both single component molecular solutions and blend solutions of these molecules with [6,6]-phenyl C70-butyric acid methyl ester (PC70BM). The blend films exhibit space-charge limited current (SCLC) hole mobilities on the order of 1×10^{-4} cm^2 V^{-1} $_S^{-1}$. Bulk heterojunction (BHJ) solar cells using these soluble molecules as donors and PC70BM as the acceptor were fabricated. Power conversion efficiencies (PCEs) of up to 2.22% under AM 1.5 G simulated 1 sun solar illumination have been achieved and external quantum efficiencies (EQEs) reach as high as ∼45%.

KEYWORDS: organic solar cells • pigments • quinacridones • molecular donors • bulk heterojunction

INTRODUCTION

The development of efficient photovoltaic cells for renewable solar energy conversion has been of great interest as it relates to the worldwide concerns of climate change and energy security (1). Solar cells based on organic materials have substantial potential for future applications due to the low cost in both materials and device fabrication. A number of new-generation solar cells are currently under investigation, including dye-sensitized solar cells (DSSCs) (2), polymer/fullerene bulk heterojunction solar cells (3), and vapor deposited small molecule solar cells (4). More recently, solution-processed solar cells using soluble small molecules have attracted great attention for their numerous attractive features, i.e., high molecular purity, reproducibility and scalable synthesis, tunable optoelectronic properties through structural control, high carrier mobility, and excellent stability (5, 6).

Simple organic dye molecules were first investigated as donor materials with devices showing PCEs of up to 1.8% (5, 6), values that are still much lower than those obtained for thermally deposited small molecule devices or polymer/fullerene devices. To develop suitable molecular donors with better device performance, a promising approach is to incorporate highly light absorbing chromophores with multiple functional groups designed to contribute to solubility, light absorption, molecular self-assembly, and carrier mobility. For instance, devices with diketopyrrolopyrrole(DPP)-thiophene derivatives as the electron donor produced PCEs of 2−4.4% (7−9). To further improve device efficiency beyond the current state-of-the-art (10), new high-performance molecular donors and a more comprehensive understanding of structure−property relationships are necessary. Herein, we report our efforts in exploring a new class of molecular donor materials based on a well-known organic pigment core of quinacridone.

Quinacridones belong to a family of organic pigments with exceptional color and weather fastness, which enable their extensive use in high-performance low-cost paints (11). Because of their high photoluminescent efficiency and good electrochemical stability, quinacridones have also been used as emitters in organic light emitting diodes (12, 13). The photoconductivity of quinacridones has been documented in a few vapor deposited organic solar cells dating back to the 1980s (14, 15). In addition, their structural nature has enabled the formation of self-assembling supramolecular

* Corresponding authors: BWMa@lbl.gov, frechet@berkeley.edu.
Received for review June 16, 2010 and accepted August 17, 2010
† These authors contributed equally to this report.
‡ Lawrence Berkeley National Laboratory.
§ University of California, Berkeley.
DOI: 10.1021/am100523g

organic semiconductors (16−18). Another unique feature of quinacridones is their fluorescence lifetime of ∼20 ns in solutions (19), which is more than an order of magnitude longer than that of typical organic donor materials (20). Therefore, quinacridone molecules may show long exciton diffusion lengths in thin films, affording enhanced exciton collection yield in bulk heterojunction devices (20). All of these properties of quinacridones have led us to explore their application in solution processed organic solar cells. To render quinacridone molecules suitable for solution processing, we have modified the quinacridone core structure by incorporating alkyl chains and thiophene units in order to improve the solubility, light absorption, and charge transporting properties. The effects of these changes in molecular structure on the physical properties and device performance were investigated. Measurements of thin film devices composed of blends of these new materials and PC70BM confirmed the importance of molecular structure with measured PCEs of 0.05% for the basic **QA** device, 1.84% for the **QA-BT** device, and 2.22% for the **QA-BTD** device.

EXPERIMENTAL SECTION

Reagents and Instrumentations. All reagents were purchased from commercial sources and used without further purification unless otherwise noted. All reactions were carried out using Schlenk line under nitrogen with anhydrous solvent. ^{1}H and ^{13}C NMR measurements were recorded using Bruker Biospin Avance II 500 MHz NMR Spectrometer with chemical shifts (δ) expressed in parts per million and splitting patterns designated as s (singlet), d (doublet), t (triplet), and m (multiplet). MALDI mass spectra were obtained using Applied Biosystems TF4800 MALDI-TOF-TOF Mass Spectrometer with α-cyano-4-hydroxycinnamic acid as matrix. Elemental analysis was carried out in a Perkin-Elmer 2400 Series II combustion analyzer. Solution UV−vis data were obtained using CARY 5000 UV−vis−NIR spectrophotometer with dilute solutions of chloroform (1×10^{-4} to 1×10^{-5} M) in quartz cells. Film UV−vis data were also recorded using the same instrument with samples on glass substrates. Photoluminescence and lifetimes measurements of the thin films were performed on a Horiba Nanolog Spectrofluorometer using the Time-correlated single photo counting (TCSPC) method for lifetime measurements in a nitrogen protecting environment. NanoLED pulsed laser-diodes of 460 nm were used to excite the QA and QA-BT samples and 560 nm for the QA-BTD sample. Cyclic voltammetry was performed using a Solartron 1285 potentiostat, wherein platinum wires act as the working and counter electrode and a silver wire as the reference electrode. Samples were prepared in dichloromethane solution with 0.1 M tetrabutylammonium hexafluorophosphate as electrolyte at a scan rate of 100 mV/s. The reference electrode was calibrated with an internal standard of ferrocene. Tapping-mode atomic force microscopy (AFM) was carried out on a Veeco Nanoscope V scanning probe microscope. Molecular geometries for **QA**, **QA-BT**, and **QA-BTD** were optimized to an energy minimum using Gaussian 09 at the DFT B3LYP level with 6-31+g(d,p) basis set. To expedite this process, we shortened alkyl chains to methyl groups on thiophene and ethyl groups on the quinacridone nitrogen. This was valid under the assumption that these alkyl chains do not contribute to the frontier molecular orbitals. Energies for the highest occupied molecular orbital (HOMO) and lowest unoccupied molecular orbital (LUMO) were obtained from the energy minimized checkpoint file. The MO surfaces were visualized at isovalue 0.2. Excitation energies and the nature of these transitions were obtained through a single-point TD-DFT calculation on the optimized geometry at the same level of theory.

Synthesis of Compounds. *N*,*N*′-Di(2-ethylhexyl)quinacridone (**QA**). Quinacridone (**1**) (5.0 g, 16.03 mmol) and tetrabutylammonium bromide (20.6 g, 64.12 mmol) were dissolved in toluene (500 mL) in a 1 L round-bottom flask. While stirring vigorously, 50% NaOH (19 mL) and 2-ethylhexyl bromide (7.1 g, 36.9 mmol) were added slowly. The resulting mixture was heated to a reflux for 26 h. The reaction was quenched with water (30 mL) and filtered. The organic layer from the filtrate was separated, and the solvent was removed under reduced pressure. The resulting crude product was purified by column chromatography eluting with dichloromethane yielding the product as red solids (2.15 g, 25%). δ_H (500 MHz, $CDCl_3$): 8.92 (s, 2H), 8.63 (d, 2H, J = 8.5 Hz), 7.78 (t, 2H, J = 7.0 Hz), 7.63 (d, 2H, J = 8.5 Hz), 7.31 (t, 2H, J = 7.5 Hz), 4.57 (s, 4H), 2.25 (m, 2H), 1.54 (m, 4H), 1.44−1.35 (m, 8H), 1.29 (m, 4H), 1.00 (t, 6H, J = 7.0 Hz), 0.88 (t, 6H, J = 7..0 Hz). MS (MALDI) *m*/*z* 537.35. CHN Anal. Calcd: C, 80.56; H, 8.26; N, 5.22. Found: C, 80.28; H, 8.37; N, 5.12.

2,9-Dibromo-*N*,*N*′-di(2-ethylhexyl)quinacridone (**3**). A stirring solution of **2** (2.15 g, 4 mmol) and NaOAc (0.85 g, 10.4 mmol) in 100 mL acetic acid was heated to reflux. A solution of Br_2 (1.45 g, 9.2 mmol) in 5 mL acetic acid was added dropwise and allowed to stir for 1 h. The mixture was cooled to room temperature, and the precipitate was collected and washed with 2% NaOH and water. The crude product was recrystallized in ethyl acetate yielding the product as red crystals (2.33 g, 83%). δ_H (500 MHz, $CDCl_3$): 8.85 (s, 2H), 8.70 (d, 2H, J = 2.5 Hz), 7.82 (dd, 2H, J = 9.5 Hz), 7.50 (d, 2H, J = 9.5 Hz), 4.54 (s, 4H), 2.18 (m, 2H), 1.52 (m, 4H), 1.45−1.37 (m, 8H), 1.29 (m, 4H), 1.00 (t, 6H, J = 7.2 Hz), 0.88 (t, 6H, J = 7.2 Hz). MS (MALDI) *m*/*z* 695.19. CHN Anal. Calcd: C, 62.26; H, 6.10; N, 4.03. Found: C, 63.17; H, 6.65; N, 3.74.

2,9-Di(2-thienyl)-*N*,*N*′-di(2-ethylhexyl)quinacridone (**4**). 3 mL of degassed toluene and 1.0 mL of degassed 2 M Na_2CO_3 (aq) were added to **3** (0.20 g, 0.29 mmol) and thiophene-2-boronic acid pinacol ester (0.14 g, 0.66 mmol), and the resulting solution was stirred and degassed for another 10 min followed by the addition of 1 drop of Aliquat 336 and $Pd(PPh_3)_4$ (0.0050 g, 0.0043 mmol). The mixture was heated to 85 °C for 4.5 h. The reaction was quenched with water (2.0 mL) and extracted with dichloromethane (10 mL). The solvent was removed under reduced pressure and the resulting crude product was purified by column chromatography eluting with dichloromethane yielding the product as red solids (0.159 g, 79%). δ_H (500 MHz, $CDCl_3$): 8.93 (s, 2H), 8.86 (d, 2H, J = 2.5 Hz), 8.04 (dd, 2H, J = 9.0 Hz), 7.76 (d, 2H, J = 9.0 Hz), 7.47 (dd, 2H, J = 3.5 Hz), 7.34 (dd, 2H,, J = 5.0 Hz), 7.16 (dd, 2H, J = 5.5 Hz), 4.60 (s, 4H), 2.28 (m, 2H), 1.54 −1.40 (m, 12H), 1.30 (m, 4H), 1.03 (t, 6H, J = 7.0 Hz), 0.89 (t, 6H,, J = 7.0 Hz). MS (MALDI) *m*/*z* 700.28.

2,9-bis(5-bromo-2-thienyl)-*N*,*N*′-di(2-ethylhexyl)quinacridone (**5**). A stirring solution of **4** (0.15 g, 0.21 mmol) in 100 mL of anhydrous chloroform was prepared. 1,3-Dibromo-5,5′-dimethyl hydantoin (0.064 g, 0.24 mmol) in 5 mL of chloroform was added dropwise at room temperature. The reaction was monitored by TLC and stopped after 4 h. The solvent was removed under reduced pressure and the crude product was purified by column chromatography eluting with 1:1 ratio of dichloromethane and hexane yielding product as red solids (0.123 g, 55%). δ_H (500 MHz, $CDCl_3$): 8.89 (s, 2H), 8.72 (d, 2H, J = 2.5 Hz), 7.90 (dd, 2H, J = 9.5 Hz), 7.64 (d, 2H, J = 9.5 Hz), 7.19 (d, 2H, J = 4.0 Hz), 7.10 (d, 2H, J = 4.0 Hz), 4.58 (s, 4H), 2.24 (m, 2H), 1.52 −1.39 (m, 12H), 1.29 (m, 4H), 1.03 (t, 6H, J = 7.0 Hz), 0.89 (t, 6H, J = 7.0 Hz).

4-bromo-7-(5-hexylthiophen-2-yl)benzo[*c*][1,2,5]thiadiazole (**7**). 15 mL of degassed toluene and 5.25 mL of degassed 2 M Na_2CO_3 (aq) were added to 4, 7-Dibromobenzo[*c*][1,2,5]thiadiazole (**6**) (0.450 g, 1.53 mmol) and 5-hexyl-2-thiophenebo-

ronic acid pinacol ester (0.450 g, 1.53 mmol), and the resulting solution was stirred and degassed for another 10 min followed by the addition of 1 drop of Aliquat 336 and $Pd(PPh_3)_4$ (0.017 g, 0.015 mmol). The mixture was heated to 85 °C for 3.5 h. The reaction was quenched with water (5 mL) and extracted with dichloromethane (10 mL). Dichloromethane was removed under reduced pressure and the resulting crude product was purified by column chromatography eluting with 1:5 ratio of dichloromethane and hexane yielding product as yellow solids (0.350 g, 60%). δ_H (500 MHz, $CDCl_3$): 7.95 (d, 1H, J = 4.0 Hz), 7.85 (d, 1H, J = 7.5 Hz), 7.67 (d, 1H, J = 7.5 Hz), 6.90 (d, 1H, J = 4.0 Hz), 2.90 (t, 2H), 1.77 (t, 2H), 1.44 (m, 2H), 1.36 (m, 4H), 0.92 (t, 3H). CHN Analysis: Calcd. C 50.39, H 4.49, N 7.35; Found: C 50.24, H 4.45, N 7.20.

2,9-Bis(5′-hexyl-2,2′-bithiophene)-*N*,*N*′-di(2-ethylhexyl)quinacridone (**QA-BT**). 2.0 mL of degassed toluene and 0.7 mL of degassed 2 M Na_2CO_3 (aq) were added to **3** (0.24 g, 0.35 mmol) and 5′-Hexyl-2,2′-bithiophene-5-boronic acid pinacol ester (0.30 g, 0.80 mmol), and the resulting solution was stirred and degassed for another 10 min followed by the addition of 1 drop of Aliquat 336 and $Pd(PPh_3)_4$ (0.0058 g, 0.0050 mmol). The mixture was heated to 85 °C for 2.5 h. The reaction was quenched with water (2.0 mL) and extracted with dichloromethane (10 mL). The organic layer was collected and the solvent was removed under reduced pressure. The resulting crude product was purified by gradient column chromatography eluting with 1:1 ratio of dichloromethane and hexane followed by dichloromethane yielding dark red solids (0.315 g, 88%). δ_H (500 MHz, CD_2Cl_2): 8.87 (s, 2H), 8.73 (d, 2H, J = 2.5 Hz), 8.00 (d, 2H, J = 10.0 Hz), 7.69 (d, 2H, J = 9.0 Hz), 7.39 (d, 2H, J = 4.5 Hz), 7.16 (d, 2H, J = 4.5 Hz), 7.10 (d, 2H, J = 4.5 Hz), 6.78 (d, 2H, J = 4.5 Hz), 4.61 (s, 4H), 2.86 (t, 4H, J = 7.5 Hz), 2.26 (m, 2H), 1.74 (m, 4H), 1.44 (m, 12H), 1.38 (m, 10H), 1.31 (m, 6H), 1.05 (t, 6H, J = 7.0 Hz), 0.95 (t, 6H, J = 7.5 Hz), 0.91 (t, 6H, J = 7.0 Hz). MS (MALDI) *m*/*z* 1033.65. CHN Anal. Calcd: C, 74.37; H, 7.41; N, 2.71. Found: C, 74.59; H, 7.49; N, 2.85.

4-(5-Hexylthiophen-2-yl)-7-(thiophen-2-yl)benzo[*c*][1,2,5]thiadiazole (**QA-BTD**). A 8 mL dioxane solution of **7** (0.30 g, 0.79 mmol), bis(pinacolato)diboron (0.23 g, 0.91 mmol), and KOAc (0.22 g, 2.24 mmol) was degassed 3 times by freeze−pump−thaw method. $Pd(dppf)Cl_2$ (0.026 g, 0.036 mmol) was added, heated to 80 °C, and stirred overnight under nitrogen. The reaction was quenched with water, and washed with ethyl acetate. The organic layer was dried over Na_2SO_4 and the solvent was removed under reduced pressure yield a red viscous liquid. The crude product (0.32 g) was confirmed by NMR, and the next step is carried out without further purification. **5** (0.25 g, 0.26 mmol) and crude product (0.30 g, 0.70 mmol) were dissolved in degassed solutions of 10 mL of toluene and 1.5 mL of 2 M Na_2CO_3 followed by the addition of 1 drop of Aliquat 336, $Pd_2(dba)_3$ (5.12 mg, 0.0056 mmol), and tri(*o*-tolyl)phosphine (4.12 mg, 0.011 mmol). The mixture was heated to 100 °C for overnight then quenched with methanol. The crude product was collected via gravity filteration and purified by gradient column chromatography eluting with chloroform followed by 3:1 ratio of chloroform and ethyl acetate. The collected product was reprecipitated in methanol yield dark red solids (0.14 g, 39%). δ_H (500 MHz, CD_2Cl_2): 8.89 (s, 2H), 8.86 (s, 2H), 8.15 (d, 2H, J = 4.0 Hz), 8.07 (d, 2H, J = 8.0 Hz), 7.97 (d, 2H, J = 3.5 Hz), 7.88 (d, 2H, J = 8.0 Hz), 7.82 (d, 2H, J = 8.0 Hz), 7.66 (d, 2H, J = 8.0 Hz), 7.54 (d, 2H, J = 4.0 Hz), 6.90 (d, 2H, J = 3.5 Hz), 4.61 (s, 4H), 2.91 (t, 4H, J = 8.0 Hz), 2.27 (m, 2H), 1.78 (m, 4H), 1.45 (m, 12H), 1.37−1.27 (m, 16H), 1.07 (m, 6H), 0.91 (m, 12H). MS (MALDI) *m*/*z* 1301.34. CHN Anal. Calcd: C, 70.12; H, 6.19; N, 6.46. Found: C, 69.82; H, 6.19; N, 6.24.

Device Fabrication and Testing. Organic solar cells were constructed with a standard device structure of ITO/PEDOT:PSS/Quinacridones:PC70BM/Al. Prepatterned ITO-coated glass substrates (R = 20 Ω/sq) were purchased from Thin Film Devices, Inc. The substrates were cleaned using the following procedure: sonication in soap solution, rinsing in deionized water, sonication in acetone and isopropanol respectively for 10 min, and UV ozone cleaning for 10 min. A thin-layer (∼30 nm) of PEDOT:PSS (Baytron PH) was spin-coated onto the ITO glass substrate at 4000 rpm for 40 s and then baked at 140 °C for 15 min in air. The photoactive layers containing the quinacridone derivatives and PC70BM in different ratios were spun cast from chloroform solutions (12−16 mg/mL) after passing through a 0.2 μm polytetrafluoroethylene filter. The thickness for all devices measured with a Dektak profilometer was between 80 and 100 nm. An Al cathode (100 nm) was then thermally evaporated under high vacuum (∼1 × 10^{-7} Torr) through a shadow mask defining an active device area of ∼0.03 cm^2. The current density−voltage (J−V) curves were measured using a Keithley 236 source-measure unit under AM 1.5 G solar illumination at 100 mW cm^{-2} (1 sun) using a Thermal-Oriel 300W solar simulator. EQEs were obtained with a monochromator and calibrated with a silicon photodiode. Hole-only devices were fabricated with a structure of ITO/PEDOT:PSS/Quinacridones/Au and fitted with the SCLC model to find the hole mobilities.

RESULTS AND DISCUSSION

Synthesis and Characterization. The pristine quinacridone is an insoluble red powder. To make materials suitable for PV application, we modified the pigment core with functional groups in order to enhance the solubility, absorption, and film forming properties. Scheme 1 summarizes the synthesis of three key compounds: **QA**, **QA-BT**, and **QA-BTD**. Starting with the pristine quinacridone (**1**) in toluene, solubilizing alkyl chains were introduced in the presence of NaOH to afford the soluble **QA** in 25% yield. This relatively low yield is due to the poor solubility of the starting quinacridone. The soluble **QA** was then used as a building block for conjugation with thiophene units. Bromination in acetic acid was carried out according to literature procedures to afford **3** in 83% yield (21). A subsequent series of Suzuki coupling afforded the desired **QA-BT** and **QA-BTD** products.

All Suzuki coupling reactions were performed under similar conditions in toluene and 2 M Na_2CO_3 solutions with Aliquat 336 added as phase-transfer catalyst. With the exception of **QA-BTD**, $Pd(PPh_3)_4$ was used as the catalyst for all reactions. **QA-BT** was obtained in 88% yield; while the more bulky and less soluble **QA-BTD** was only obtained in 39% yield. In the conversion of **7** to boronic acid pinacol ester, no further purification was performed because of the product's sensitivity to degradation in silica gel. Once the ^{1}H NMR verified the crude product (purity > ∼96%), the preparation proceeded with the next step. All the synthesized compounds are soluble in common organic solvents, e.g., dichloromethane, chloroform, toluene, and THF. The final products were fully characterized by ^{1}H NMR spectroscopy, elemental analysis, and MALDI mass spectrometry.

Physical Properties. The UV−vis absorption spectra shown in Figure 1 were recorded in chloroform solutions and in thin films on glass substrates for all three compounds. The diethylhexyl functionalized **QA** shows a similar spectrum with absorbance maximum corresponding to a $\pi \rightarrow \pi^*$ transition at around 520 nm in both solution and thin film,

Scheme 1. Synthetic Routes to the Compounds QA, QA-BT, and QA-BTD

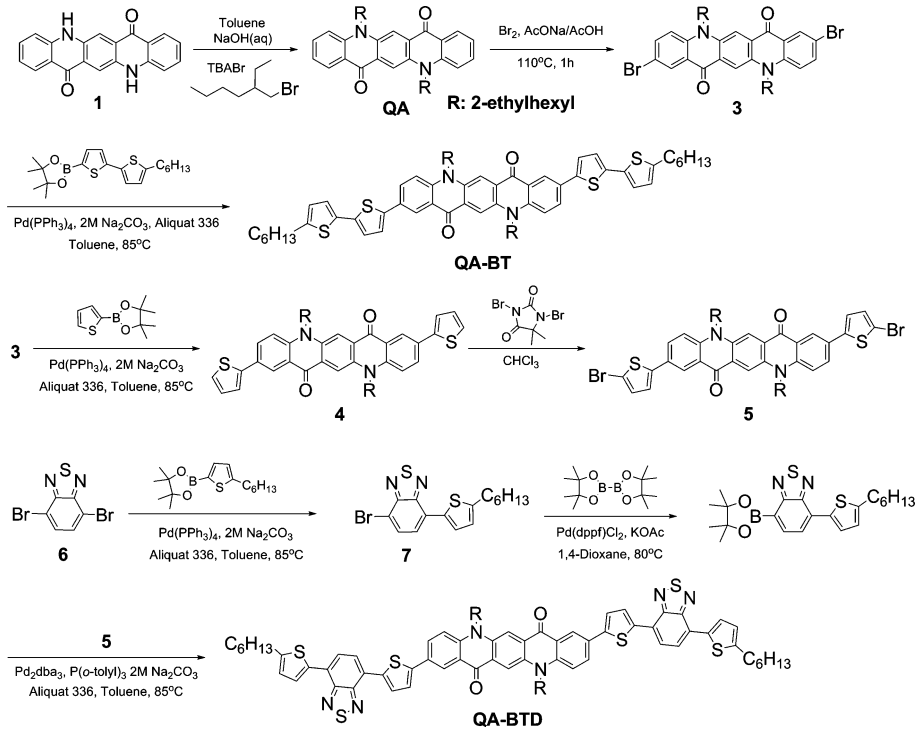

suggesting little-to-no molecular aggregation in the solid state. This is in sharp contrast with what is observed in analogous experiments with the pristine quinacridone, which is yellow in solution but reddish to violet in the solid state due to extensive formation of intermolecular hydrogen bonds (22). Following the incorporation of thiophene units, either BT or BTD, the absorption bands extend from ~550 nm to lower energy levels of ~600 nm in solutions and the absorption intensities in high energy levels (350−450 nm) increase significantly, affording better overlaps with the solar spectrum. A pronounced absorption peak at around 400 nm with exceptional extinction coefficients of $\sim 1 \times 10^6$ cm^{-1} M^{-1} was observed in **QA-BT** solution, which can be assigned to the $\pi \rightarrow \pi^*$ transition of the incorporated bithiophene units. It is believed that the quinacridone core promotes the light absorption capability of bithiophenes by enhancing the conjugation and affording planar molecular conformation (23). The optical bandgaps obtained from the thin film absorption edges are 2.25 eV for **QA**, 2.09 eV for **QA-BT**, and 1.94 eV for **QA-BTD**. When comparing solution absorption to film absorption, **QA** and **QA-BT** show little change in the absorbance maximum, whereas a pronounced shift is observed in **QA-BTD**. The large shift in **QA-BTD** can be attributed to its strong molecular packing via long planar molecular structures in the solid state. And the rigid molecular geometry allows for better electronic interaction between the quinacridone core and benzothiadiazole moieties, resulting in enhanced internal charge transfer (24).

The electrochemical properties of these compounds were investigated using cyclic voltammetry. Figure 2a shows the CV curves for the three compounds in anhydrous dichloromethane solution. The oxidation and reduction potentials relative to an internal ferrocene/ferrocenium redox couple (−5.1 eV vs vacuum) (25) are summarized in Table 1. As the molecular conjugation length increases, the HOMO levels shift from −5.8 eV for **QA** to −5.64 eV for **QA-BT** and −5.55 eV for **QA-BTD**, and the LUMO levels goes from −3.27 eV for **QA** to −3.34 eV for **QA-BT** and −3.42 eV for **QA-BTD**. This translates into reductions in electrochemical bandgaps from 2.53 eV for **QA** to 2.30 eV for **QA-BT** and 2.13 eV for

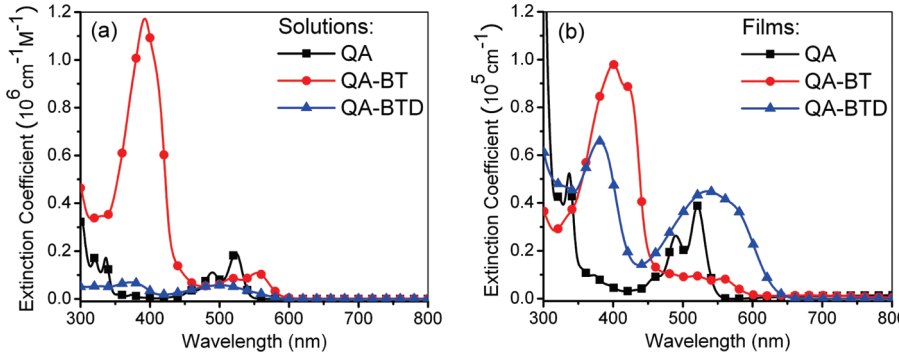

FIGURE 1. Absorption spectra of (a) chloroform solutions and (b) thin films on glass substrates of QA, QA-BT, and QA-BTD.

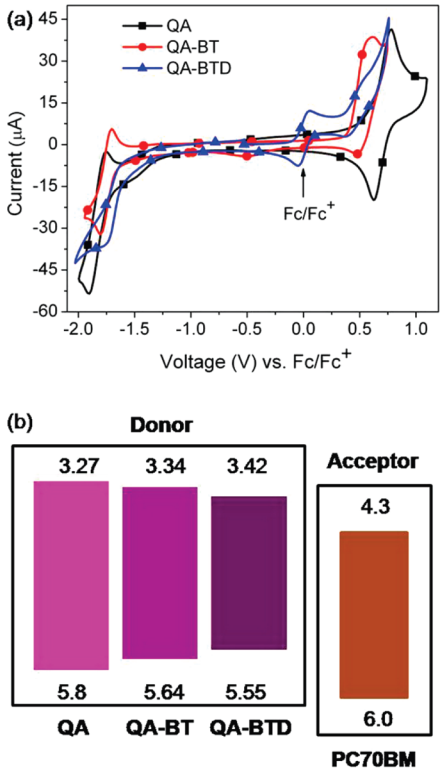

FIGURE 2. (a) Cyclic voltammetry curves of QA, QA-BT, and QA-BTD in dichloromethane solution, and the internal potential reference of Fc/Fc+ peak is also shown together in the blue line; (b) energy levels diagram of the three synthesized compounds and PC70BM.

QA-BTD, which is consistent with the trend observed for the optical bandgaps. These deep lying HOMO levels and sufficient LUMO offsets (>0.8 eV), as shown in Figure 2b, allow these new compounds to act as electron donors when they are coupled with the acceptor PC70BM, which possesses a HOMO level of −6.0 eV and a LUMO level of −4.3 eV (26).

To gain a deeper understanding of the effects of the attached BT and BTD units on the electronic properties observed in the UV−vis and CV experiments, DFT calculations for the methyl analogs of these three compounds were carried out. The molecular geometries, surface plots, and HOMO and LUMO energy levels are displayed in Figure 3. Remarkable variations in the surface plots are observed for these compounds, implying very different characteristics of excited states and transitions. Specifically, the HOMO for both **QA-BT** and **QA-BTD** display well delocalized orbitals across the quinacridone core and attached BT and BTD units. This enhanced conjugation leads to the shallower HOMO levels of approximately −4.9 eV for **QA-BT** and **QA-BTD** compared to that of **QA** (approximately −5.2 eV). In contrast, the LUMOs for **QA-BT** and **QA-BTD** are localized in different positions with significantly different energy levels, i.e. in the quinacridone core for **QA-BT** (approximately −2.2 eV) and in the BTD unit for **QA-BTD** (approximately −2.6 eV). This is a result of the relatively strong electron-withdrawing characteristics of benzothiadiazole as compared to the quinacridone core (25). Therefore, the origins of the lowest absorption bands can be assigned to different transitions, i.e., (QA-BT)$\pi \rightarrow$ (QA)π^* for **QA-BT** and (QA-BTD)$\pi \rightarrow$ (BTD)π^* for **QA-BTD**. In other words, **QA-BT** possesses a donor−acceptor−donor (D−A−D) type of conjugated system, whereas **QA-BTD** is an acceptor−donor−acceptor (A−D−A) system. This difference in the characteristics of LUMOs can clearly elucidate that **QA-BTD** has much higher absorption intensities than **QA-BT** in the low energy levels centered at ∼550 nm and lower intensities in the high energy levels centered at ∼400 nm in the solid state. The enhanced conjugation and the change in transitions result in the bandgaps for the three compounds to decrease in the order of **QA** > **QA-BT** > **QA-BTD**.

The change in molecular structure also significantly influences the photoluminescence properties of these compounds, i.e., emission wavelengths and lifetimes. As shown in Figure 4a, the emission spectra for thin films of **QA**, **QA-BT**, and **QA-BTD** exhibit fluorescence peaks at 578, 626, and 695 nm, respectively. This trend is consistent with the results of the absorption, CV, and DFT calculations. Figure 4b shows the decay curves for the emission of the three compounds in thin films. The lifetimes decrease from 11.19 ns for **QA** to 4.33 ns for **QA-BT** and 1.3 ns for **QA-BTD** that we observe can be explained by (i) the change in the characteristics of excited states and transitions and (ii) the increase of nonradiative decay with decreasing bandgap based on the Energy Gap Law (27). Nevertheless, these lifetimes are still significantly longer than those measured for a typical poly(3-hexylthiophene) (P3HT) film (28).

Organic Solar Cells. Solution processed bulk heterojunction (BHJ) solar cells were fabricated with these new quinacridone-based molecules as the electron donor and PC70BM as the acceptor with a simple device structure of ITO/PEDOT:PSS(30 nm)/Blend(∼90 nm)/Al(100 nm), as shown in Figure 5a. We have carefully screened various processing solvents, blend ratios and film thicknesses to achieve optimized conditions for the device fabrication. The film morphology, charge carrier mobility, and device characteristics were thoroughly examined. Highest performance devices were obtained by using chloroform as the processing solvent with different weight ratios for the three compounds used in conjunction with PC70BM, i.e., 1:3 for **QA**/PC70BM,

Table 1. Summary of the Physical Properties of Compounds QA, QA-BT, and QA-BTD

films	E_{opt} (eV)[a]	E^{ox} (V)[b]	E^{red} (V)[b]	HOMO (eV)[c]	LUMO (eV)[d]	emission peak (nm)	lifetimes (ns)	u_{hole} ($cm^2\ V^{-1}\ s^{-1}$)[e]
QA	2.25	0.70	−1.83	−5.8	−3.27	578	11.19	3.96×10^{-6}
QA-BT	2.09	0.54	−1.76	−5.64	−3.34	626	4.33	5.58×10^{-5}
QA-BTD	1.94	0.45	−1.68	−5.55	−3.42	695	1.3	5.25×10^{-5}

[a] Estimated from the absorption edge of thin films. [b] Determined by cyclic voltammetry and calculated with reference to ferrocene (5.1 eV vs vacuum). [c] $E_{HOMO} = -(E^{ox} + 5.1)$ eV. [d] $E_{LOMO} = -(E^{red} + 5.1)$ eV. [e] Mobilities calculated according to the SCLC model.

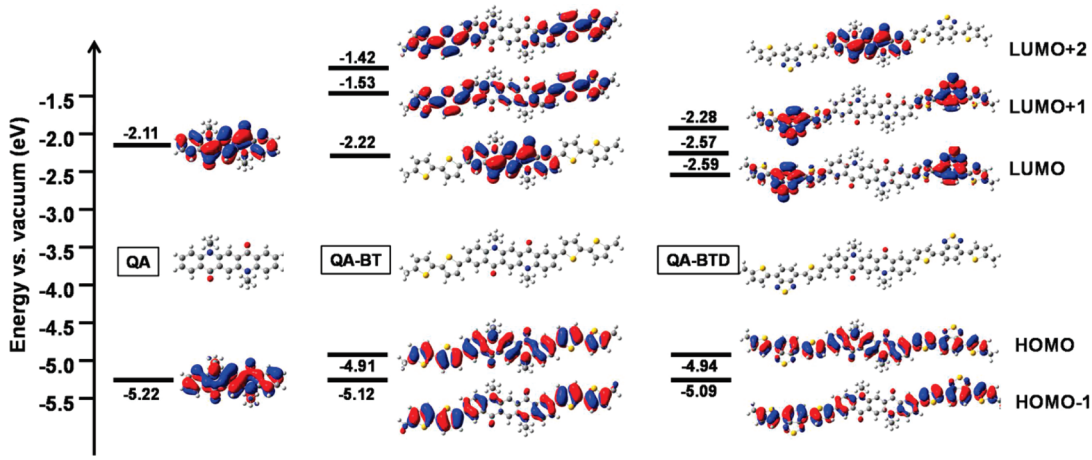

FIGURE 3. HOMO and LUMO surface plots for QA, QA-BT, and QA-BTD.

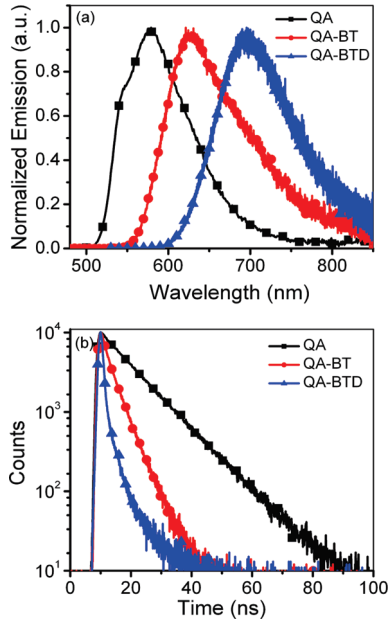

FIGURE 4. (a) Photoluminescence spectra of films on glass substrates and (b) decay curves of these emissions for QA, QA-BT, and QA-BTD.

1:2.5 for **QA-BT**/PC70BM, and 1:2 for **QA-BTD**/PC70BM. Because **QA-BTD** has slightly higher molecular weight than **QA-BT**, the molecular ratios in those devices were very similar indeed. Thermal annealing had a negative effect on device performance, a finding that is not surprising if a suitable phase separated morphology is already obtained in the films "as-cast".

Tapping mode atomic force microscopy (AFM) was used to investigate the morphology of these optimized blend films, with images shown in Figure 5b–d. The root-mean-square (rms) roughness of the blend films changes significantly from 7.2 nm for **QA**/PC70BM to 0.94 nm for **QA-BT**/PC70BM and 0.37 nm for **QA-BTD**/PC70BM. In addition, the phase-separated domain size decreases from **QA**/PC70BM to **QA-BT**/PC70BM and **QA-BTD**/PC70BM. This demonstrates that the choice of side arms has a dramatic effect on film morphology as it controls the miscibility of the functionalized quinacridones with PC70BM. It is likely that the smoother film of **QA-BTD** with its finer phase separation would lead to higher device performance than films of the other two compounds.

The charge-carrier mobilities of thin films were measured using the space-charge-limited-current (SCLC) method. Hole-only devices with the structure of ITO/PEDOT:PSS/Thin film/Au were fabricated, wherein the thin film contains either QA compounds as a single component or blends of QA compound/PC70BM in the ratios listed described above. The neat films showed modest hole mobilities on the order of 1×10^{-5} cm^2 V^{-1} $_S$ $^{-1}$, as listed in Table 1. The introduction of PC70BM acceptor had a positive influence on the hole mobility (29), with higher mobility values on the order of 1×10^{-4} cm^2 V^{-1} $_S$ $^{-1}$, as listed in Table 2.

Figure 6a shows the current density–voltage (J–V) curves for the optimized devices under AM 1.5 G simulated solar illumination with an intensity of 100 mW cm^{-2}. Table 2 summarizes the device characteristics, including short circuit

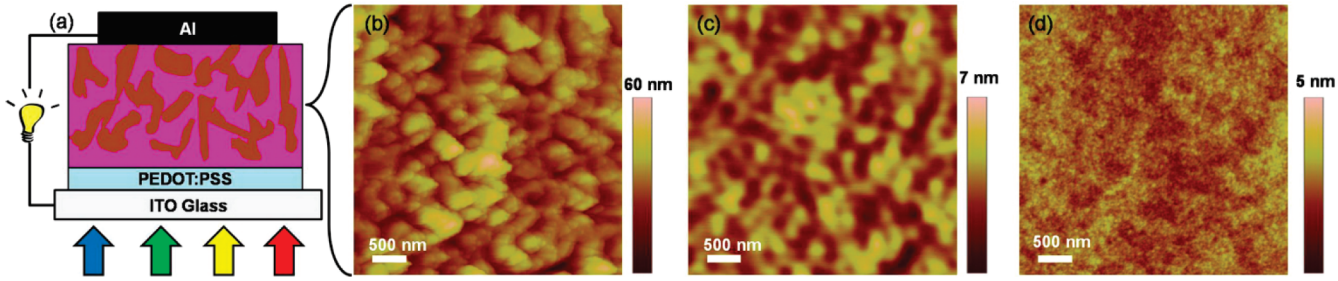

FIGURE 5. (a) Schematic device architecture for a BHJ solar cell; and tapping mode AFM topographical images of actual blends of (b) QA/PC70BM (1:3), (c) QA-BT/PC70BM (1:2.5), and (d) QA-BTD/PC70BM (1:2).

Table 2. Summary of the Film Properties and Device Performance for the Blends of Quinacridone-Based Molecules and PC70BM

active layer (w/w)	thickness (nm)	rsm (nm)	u_{hole} ($cm^2\ V^{-1}\ s^{-1}$)	V_{oc} (V)	J_{sc} ($mA\ cm^{-2}$)	FF	PCE (%)
QA:PC70BM (1:3)	91	7.2	2.33×10^{-4}	0.20	−0.94	0.28	0.05
QA-BT:PC70BM (1:2.5)	94	0.94	3.29×10^{-4}	0.80	−5.67	0.40	1.84
QA-BTD:PC70BM (1:2)	82	0.37	2.07×10^{-4}	0.72	−8.87	0.35	2.22

current (J_{sc}), open circuit voltage (V_{oc}), fill factor (*FF*), and power conversion efficiency (PCE) for these optimized devices. The **QA** devices barely worked as a photovoltaic cell with very low current density and open circuit voltage, which is likely due to the poor film morphology with large microphase separation as shown in Figure 5b. **QA-BT** and **QA-BTD** devices achieved reasonably high open circuit voltages of 0.80 and 0.72 V, respectively. The slightly higher V_{oc} for **QA-BT** is attributed to its deeper HOMO level than that of **QA-BTD**. Short-circuit current densities of 5.67 and 8.87 mA cm^{-2} were obtained for the **QA-BT** device and **QA-BTD** device, respectively. The much higher current density for the **QA-BTD** device is likely a result of the better absorption property and finer film morphology. It is also likely that the change of molecular geometry from D−A−D type for **QA-BT** to A−D−A for **QA-BTD** increases the exciton dissociation efficiency and decreases the charge recombination at the donor/acceptor interfaces (30). Figure 6b shows the external quantum efficiencies (EQEs) for these two devices. Similar EQEs were achieved for the two devices in the regions of 300−400 nm and beyond 680 nm, which are mainly contributed by the PC70BM acceptor. However, in the 420−600 nm region, EQEs of exceeding 40% were realized for the **QA-BTD** device, whereas only 30% was realized for **QA-BT**; the EQEs in this region are mainly contributed by the donor materials. Fill factors of 0.40 and 0.35 were achieved for the **QA-BT** and **QA-BTD** device, respectively, which are relatively low when compared to those of typical polymer/fullerene solar cells. Possible issues accounting for the low fill factors include the nonideal morphology and organic/electrode interfacial contact problems. These issues will be addressed in future experiments. Overall, we have achieved PCEs of 0.05% for **QA**/PC70BM, 1.84% for **QA-BT**/PC70BM, and 2.22% for **QA-BTD**/PC70BM. To the best of our knowledge, the value of 2.22% is among the highest efficiencies for "as-cast" small molecule based BHJ solar cells reported in the literature to date.

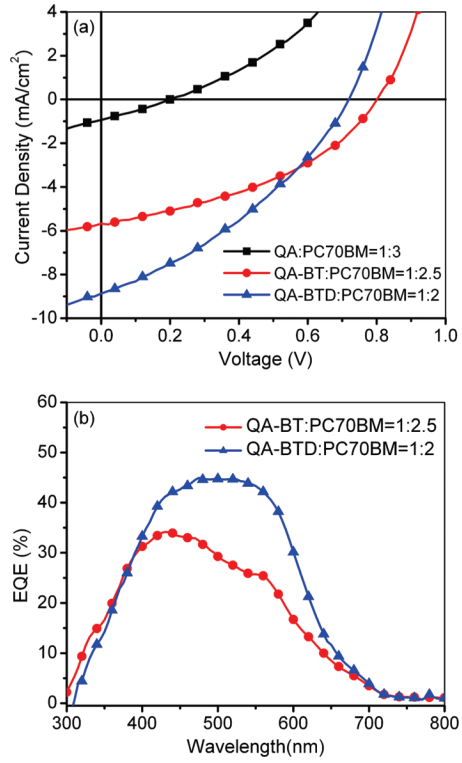

FIGURE 6. (a) Current density−voltage (*J*−*V*) characteristics of devices with three compounds as donor and PC70BM as acceptor under AM 1.5 G, 100 mW cm^{-2}; and (b) EQE spectra for devices based on QA-BT and QA-BTD.

CONCLUSIONS

In summary, we have designed, synthesized, and characterized a series of soluble pigment-based photovoltaic molecules. The pristine insoluble quincridone molecules were functionalized with solubilizing alkyl chains and various thiophene units, leading to solution-processable materials with suitable properties for photovoltaic application. The use of these multifunctional molecules as electron donors was demonstrated in BHJ devices with PC70BM as the electron acceptor. Solution-processed thin films show bicontinuous nanophase separated morphology, which is feasible for exciton dissociation and charge transport. Power conversion efficiencies of up to 2.2% with external quantum efficiencies exceeding 45% have been achieved under an AM 1.5 G simulated solar illumination. Our work clearly suggests that low-cost pigment-based molecular materials have potential for use in highly efficient organic solar cells. Ongoing research to further improve the device performance of this class of materials lies in optimizing the light absorption, charge transporting property, and film morphology via molecular structural control and device engineering.

Acknowledgment. This work was performed at the Molecular Foundry, Lawrence Berkeley National Laboratory, and was supported by the Office of Science, Office of Basic Energy Sciences, Scientific User Facilities Division, and the Materials Sciences and Engineering Division, U.S. Department of Energy, under Contract DE-AC02-05CH11231.

REFERENCES AND NOTES

(1) Lewis, N. S. *Science* **2007**, *315*, 798–801.
(2) Oregan, B.; Gratzel, M. *Nature* **1991**, *353*, 737–740.
(3) Yu, G.; Gao, J.; Hummelen, J. C.; Wudl, F.; Heeger, A. J. *Science* **1995**, *270*, 1789–1791.
(4) Tang, C. W. *Appl. Phys. Lett.* **1986**, *48*, 183–185.
(5) Lloyd, M. T.; Anthony, J. E.; Malliaras, G. G. *Mater. Today* **2007**, *10*, 34–41.
(6) Roncali, J. *Acc. Chem. Res.* **2009**, *42*, 1719–1730.

(7) Tamayo, A. B.; Walker, B.; Nguyen, T. Q. *J. Phys. Chem. C* **2008**, *112*, 11545–11551.
(8) Tamayo, A. B.; Dang, X. D.; Walker, B.; Seo, J.; Kent, T.; Nguyen, T. Q. *Appl. Phys. Lett.* **2009**, *94*, 103301–103303.
(9) Walker, B.; Tomayo, A. B.; Dang, X. D.; Zalar, P.; Seo, J. H.; Garcia, A.; Tantiwiwat, M.; Nguyen, T. Q. *Adv. Funct. Mater.* **2009**, *19*, 3063–3069.
(10) Chen, H. Y.; Hou, J. H.; Zhang, S. Q.; Liang, Y. Y.; Yang, G. W.; Yang, Y.; Yu, L. P.; Wu, Y.; Li, G. *Nat. Photonics* **2009**, *3*, 649–653.
(11) Labana, S. S.; Labana, L. L. *Chem. Rev.* **1967**, *67*, 1–18.
(12) Wakimoto, T.; Yonemoto, Y.; Funaki, J.; Tsuchida, M.; Murayama, R.; Nakada, H.; Matsumoto, H.; Yamamura, S.; Nomura, M. *Synth. Met.* **1997**, *91*, 15–19.
(13) Wang, J.; Zhao, Y. F.; Dou, C. D.; Sun, H.; Xu, P.; Ye, K. Q.; Zhang, J. Y.; Jiang, S. M.; Li, F.; Wang, Y. *J. Phys. Chem. B* **2007**, *111*, 5082–5089.
(14) Tomida, M.; Kusabayashi, S.; Yokoyama, M. *Chem. Lett.* **1984**, 1305–1308.
(15) Manabe, K.; Kusabayashi, S.; Yokoyama, M. *Chem. Lett.* **1987**, 609–612.
(16) Ye, K. Q.; Wang, J.; Sun, H.; Liu, Y.; Mu, Z. C.; Li, F.; Jiang, S. M.; Zhang, J. Y.; Zhang, H. X.; Wang, Y.; Che, C. M. *J. Phys. Chem. B* **2005**, *109*, 8008–8016.
(17) Trixler, F.; Market, T.; Lackinger, M.; Jamitzky, F.; Heckl, W. M. *Chem.—Eur. J.* **2007**, *13*, 7785–7790.
(18) Wang, J.; Zhao, Y. F.; Zhang, J. H.; Zhang, J. Y.; Yang, B.; Wang, Y.; Zhang, D. K.; You, H.; Ma, D. G. *J. Phys. Chem. C* **2007**, *111*, 9177–9183.
(19) Smith, J. A.; West, R. M.; Allen, M. *J. Fluoresc.* **2004**, *14*, 151–171.
(20) Peumans, P.; Yakimov, A.; Forrest, S. R. *J. Appl. Phys.* **2003**, *93*, 3693–3723.
(21) Liu, J.; Gao, B. X.; Cheng, Y. X.; Xie, Z. Y.; Geng, Y. H.; Wang, L. X.; Jing, X. B.; Wang, F. S. *Macromolecules* **2008**, *41*, 1162–1167.
(22) Paulus, E. F.; Leusen, F. J. J.; Schmidt, M. U. *CrystEngComm* **2007**, *9*, 131–143.
(23) DiCesare, N.; Belletete, M.; Donat-Bouillud, A.; Leclerc, M.; Durocher, G. *Macromolecules* **1998**, *31*, 6289–6296.
(24) Biniek, L.; Chochos, C. L.; Leclerc, N.; Hadziioannou, G.; Kallitsis, J. K.; Bechara, R.; Leveque, P.; Heiser, T. *J. Mater. Chem.* **2009**, *19*, 4946–4951.
(25) Zhao, X. Y.; Piliego, C.; Kim, B.; Poulsen, D. A.; Ma, B. W.; Unruh, D. A.; Frechet, J. M. J. *Chem. Mater.* **2010**, *22*, 2325–2332.
(26) Park, S. H.; Roy, A.; Beaupre, S.; Cho, S.; Coates, N.; Moon, J. S.; Moses, D.; Leclerc, M.; Lee, K.; Heeger, A. *J. Nat. Photonics* **2009**, *3*, 297–2U5.
(27) Englman, R.; Jortner, J. *Mol. Phys.* **1970**, *18*, 145–164.
(28) Xu, B.; Holdcroft, S. *Thin Solid Films* **1994**, *242*, 174–177.
(29) Andersson, L. M.; Inganas, O. *Appl.Phys. Lett.* **2006**, *88*, 82103–82105.
(30) Holcombe, T. W.; Woo, C. H.; Kavulak, D. F. J.; Thompson, B. C.; Frechet, J. M. J. *J. Am. Chem. Soc.* **2009**, *131*, 14160–14161.

AM100523G